Int. J. Solids Structures Vol. 23, No 5, pp. 581 597, 1987
Printed in Great Britain

0020 7683/87 $3.00 + 00

SLIDING CONTACT STRESSES IN A TWO-DIMENSIONAL LAYERED ELASTIC HALF-SPACE

R. B. KING and T. C. O'SULLIVAN
IBM Almaden Research Center, 650 Harry Road, San Jose, CA 95120-6099, U.S.A.

(*Received* 19 *February* 1986; *in revised form* 25 *April* 1986)

Abstract—Knowledge of the contact stress state in layered media is important for quantitative understanding of the mechanical reliability of the media. The two-dimensional quasi-static stress analysis of a layer on an elastic half-space under combined normal and sliding cylindrical contact is studied. Results are presented for the stresses in both the layer and half-space and contrasted with the case of a homogeneous medium.

NOTATION

a	contact zone half-width
a_0	contact zone half-width for $E_1 = E_2$
E_1, ν_1	Young's modulus, Poisson's ratio for layer
E_2, ν_2	Young's modulus, Poisson's ratio for substrate
f	coefficient of friction
h	layer thickness
$p(x)$	pressure under indenter
p_0	pressure under center of indenter for $E_1 = E_2$
L	indenter load
$q(x)$	shear traction under indenter
u_i	displacement vector
φ	Airy's stress function
σ_{ij}	stress tensor
ω	Fourier transform variable.

INTRODUCTION

Analysis of the stress state in layered media under combined sliding and normal contact is important for assessing mechanical reliability. Applications include protective coatings, layered composite media, and thin films. The quasi-static analysis presented in this paper permits quantifying the effects of sliding contact on a layered elastic medium.

The combined sliding and normal contact stress analysis of layered media has not previously been performed. Theoretical results are presented for sliding contact on a layered medium and contrasted with the case of a homogeneous medium. The cylindrical indenter is assumed to be rigid and of circular cross-section in this study. The analysis can be extended in a straightforward manner to include elastic indenters. The sliding contact problem is modelled as two-dimensional with both in-plane and anti-plane sliding contact being considered.

Quasi-static sliding contact stress analysis has previously been reported for the case of a cylindrical indenter contacting an elastic half-space with no layer[1, 2]. Contour plots of the Von Mises stress in Ref. [2] exhibit a maximum value at a subsurface position directly below the indenter for low coefficients of friction, and this maximum migrates to the surface for higher coefficients of friction. The equivalent analysis of a spherical indenter contacting a homogeneous half-space was also performed in Ref. [2] with similar results. No analogous study has been performed for layered media. The normal contact problem (i.e. with no sliding) for layered media has previously been investigated. The elasticity theory necessary to solve for the stress state under prescribed axisymmetric normal surface loading for a single layer on a half-space was developed by Burmister[3] and extended by Chen[4] to axisymmetric and non-axisymmetric normal loading on multilayered half-spaces. Chen and Engel[5] used a least-squares approach to solve the normal contact problem, and presented the pressure profile under indenters of various geometries for a

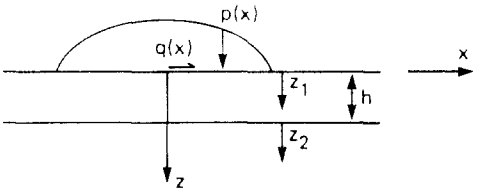

Fig. 1. Contact problem geometry.

half-space with a single layer. Gupta and Walowit[6] investigated the normal contact problem in plane strain for a single layer on a half-space. They developed a plane-strain theory for arbitrary surface loading, and used an integral equation approach to study the normal contact problem based on Ref. [7]. Results were given in Ref. [6] for the pressure distribution under a cylindrical indenter and parameter studies were performed for the effect of relative stiffness of the indenter, layer, and half-space. Results have not been presented for the subsurface stress distribution caused by the normal contact on a layered medium in either the two- or three-dimensional cases. The theory needed for arbitrary surface loading in plane strain was previously developed in Ref. [8], although it was not utilized to study the sliding contact problem.

In the present work, a detailed analysis of the subsurface stresses in plane strain due to normal and sliding contact on a half-space with a single layer has been performed. In addition anti-plane sliding, important for some geometries, is studied here and an approximate theory treating the layer as a membrane is given.

IN-PLANE STRESS ANALYSIS

An important ingredient necessary to solve the contact problem is an elasticity solution for arbitrary boundary loading on the surface of a half-space. The approach in Ref. [6] will be followed for the plane-strain case. In the layer the stresses and displacements are taken as functions of x and z_1 while in the half-space they are functions of x and z_2 (Fig. 1). The normal and tangential tractions are prescribed in a certain region $|x| \leq a$ on the surface $z_1 = 0$, and outside this region the surface is traction-free

$$\begin{aligned} \sigma_{zz}^{(1)}(x,0) &= -p(x), |x| \leq a \qquad \sigma_{zz}^{(1)}(x,0) = 0, |x| > a \\ \sigma_{xz}^{(1)}(x,0) &= -q(x), |x| \leq a \qquad \sigma_{xz}^{(1)}(x,0) = 0, |x| > a \end{aligned} \tag{1}$$

The interface between the layer and the half-space is required to have continuous tractions and displacements for all values of x

$$\begin{aligned} \sigma_{xz}^{(1)}(x,h) &= \sigma_{xz}^{(2)}(x,0) \qquad u^{(1)}(x,h) = u^{(2)}(x,0) \\ \sigma_{zz}^{(1)}(x,h) &= \sigma_{zz}^{(2)}(x,0) \qquad w^{(1)}(x,h) = w^{(2)}(x,0) \end{aligned} \tag{2}$$

Superscripts (1) and (2) refer to the layer and half-space, respectively. There is in addition a boundedness condition for the solution in the half-space for large x and z_2. The stresses are next expressed in terms of Airy's stress function, φ. Equilibrium is thus automatically satisfied, while elastic compatibility requires that the stress function be biharmonic[9]

$$\nabla^4 \varphi = 0. \tag{3}$$

The solution is obtained by taking the Fourier transform of φ and the stresses and displacements with respect to x using the definitions

$$\bar{\varphi} = \int_{-\infty}^{\infty} \varphi \, e^{i\omega x} \, dx, \qquad \bar{\sigma}_{zz} = \int_{-\infty}^{\infty} \sigma_{zz} \, e^{i\omega x} \, dx, \tag{4}$$

etc. Equation (3) then reduces to an ordinary differential equation, the solution of which is

$$\begin{aligned}\bar{\varphi}^{(1)} &= (A_1 + B_1 z_1)e^{-|\omega|z_1} + (C_1 + D_1 z_1)e^{|\omega|z_1} \\ \bar{\varphi}^{2} &= (A_2 + B_2 z_2)e^{-|\omega|z_2}\end{aligned} \tag{5}$$

Here $\bar{\varphi}^{(1)}$ and $\bar{\varphi}^{(2)}$ are the solutions in the layer and substrate, respectively. Enforcement of the two boundary and four interface conditions then leads to a linear system of six equations for the six coefficients A_1, B_1, C_1, D_1, A_2, B_2 in the form

$$[A]\begin{bmatrix} A_1 \\ B_1 \\ C_1 \\ D_1 \\ A_2 \\ B_2 \end{bmatrix} = \begin{bmatrix} \bar{p} \\ \bar{q} \\ 0 \\ 0 \\ 0 \\ 0 \end{bmatrix} \tag{6}$$

where $\bar{p}$ and $\bar{q}$ are the Fourier transforms of the normal pressure and shear traction on the surface, respectively. (The coefficient matrix A is given in Ref. [6].) For a prescribed boundary loading $p(x)$ and $q(x)$, the numerical solution procedure is to determine $\bar{p}$ and $\bar{q}$ (which can be done analytically for simple enough loadings), then solve eqn (6) at a number of discrete frequencies, followed by numerical inverse transformation to obtain the stresses and displacements. The integrand of the Fourier inversion for the displacements becomes singular as ω tends to zero. This is the manifestation in the Fourier transform solution of singular behavior of displacements in two-dimensional contact problems[10]. This problem is eliminated if, instead of the absolute displacement $w^{(1)}(x, z_1)$, we compute the relative displacement $w^{(1)}(x, z_1) - w^{(1)}(x_r, z_1)$, where x_r is a reference point. As discussed below, it is the relative displacement which is needed in any case in solving the contact problem.

ANTI-PLANE STRESS ANALYSIS

For anti-plane sliding the out-of-plane shear traction component on the surface is given by

$$\sigma_{yz}^{(1)}(x, 0) = -fp(x) \equiv r(x). \tag{7}$$

Given this prescribed boundary loading, the stresses are solved for in the medium as follows. The anti-plane strain case is uncoupled from the in-plane case. The only non-zero displacement component is $v \equiv u_y$, which is a function of x and z only. Equilibrium requires that v be a harmonic function. The boundary condition is given by eqn (7) under the indenter while the boundary is traction-free elsewhere. The interface conditions are that v and σ_{yz} are continuous. Taking the Fourier transform of the displacements and stresses results in the solution

$$\begin{aligned}\bar{v}^{(1)} &= A e^{-|\omega|z_1} \\ \bar{v}^{(2)} &= B e^{-|\omega|z_2} + C e^{|\omega|z_2}\end{aligned} \tag{8}$$

The Fourier transform of the boundary and interface conditions then give three equations for the unknowns A, B, and C, which are solved for explicitly. Knowing A, B, and C, the displacement v and its spatial derivatives can be calculated, and the Fourier transform of the stresses are determined from the constitutive relations

$$\sigma_{yz} = \mu\frac{\partial v}{\partial z}, \qquad \sigma_{xy} = \mu\frac{\partial v}{\partial x} \tag{9}$$

where μ is the shear modulus. The results for the anti-plane shear stress are

$$\bar{\sigma}_{yz}^{(1)} = \left\{ -\frac{t^2}{\bar{\mu} - t^2} e^{-|\omega| z_1} + \frac{\bar{\mu}}{\bar{\mu} - t^2} e^{|\omega| z_1} \right\} \bar{P}(\omega)$$

$$\bar{\sigma}_{yz}^{(2)} = -\mu' \left\{ \frac{2t}{(1 - \mu') - (1 + \mu') t^2} e^{-|\omega| z_2} \right\} \bar{P}(\omega) \tag{10}$$

where $t = e^{|\omega| h}$, $\mu' = \mu_2/\mu_1$ and $\bar{\mu} = (1 - \mu')/(1 + \mu')$. As in the in-plane case, the numerical solution procedure is to the first Fourier transform the applied shear tractions on the boundary analytically. The stresses are then determined using eqns (10) by numerical inverse Fourier transformation.

MEMBRANE APPROXIMATION

For the case of very thin layers (where the layer thickness is much smaller than the contact zone) a simplified theory can be derived. In this case the layer acts essentially as a membrane attached to a half-space. The normal stress σ_{zz} and the shear stress σ_{xz} are assumed to be the same as in the non-layered case, and it is assumed that the layer does not appreciably alter the pressure profile. Hence the pressure profile from the non-layered contact solution is prescribed. The membrane stress component σ_{xx} is significantly affected by the presence of the layer, however.

The equation of equilibrium for a membrane subjected to shear tractions q_1 and q_2 on its top and bottom surfaces, respectively, is

$$h \frac{\partial \sigma_{xx}^{(1)}(x)}{\partial x} = -q_1(x) - q_2(x). \tag{11}$$

The membrane also has pressure prescribed on its top surface. The stress σ_{zz} is assumed to be constant with z in the membrane, so $\sigma_{zz}^{(1)}(x, z) = -p(x)$. From the isotropic elastic constitutive relation, σ_{xx} is given by

$$\sigma_{xx}^{(1)}(x) = \frac{E_1}{(1 - \nu_1^2)} \frac{\partial u^{(1)}(x)}{\partial x} - \frac{\nu_1}{(1 - \nu_1)} p(x). \tag{12}$$

Here $u^{(1)}$ is the horizontal displacement component in the membrane and E_1, ν_1 are Young's modulus and Poisson's ratio in the membrane. Substituting in eqn (11) results in

$$\frac{E_1 h}{(1 - \nu_1^2)} \frac{\partial^2 u^{(1)}}{\partial x^2} = \frac{h \nu_1}{(1 - \nu_1)} \frac{\partial p}{\partial x} - q_1 - q_2. \tag{13}$$

The half-space solution is expressed in terms of Airy's stress function as presented above. The Fourier transform of $\varphi^{(2)}$ is then given by

$$\bar{\varphi}^{(2)} = (A + B z_2) e^{-|\omega| z_2}. \tag{14}$$

The interface conditions at $z_2 = 0$ are

$$\begin{aligned} \sigma_{zz}^{(2)}(x, 0) &= -p(x) \\ \sigma_{xz}^{(2)}(x, 0) &= q_2(x) \\ u^{(2)}(x, 0) &= u^{(1)}(x). \end{aligned} \tag{15}$$

Equations (11)–(15) may be reduced to three equations that are solved for $\bar{u}^{(1)}$, A and B. The stress σ_{xx} can then be solved for in the layer and substrate by numerical inverse Fourier transformation. As shown below, results from the full two-dimensional theory indicate that the membrane theory is a good approximation when the ratio, a/h, of the contact zone half width to layer thickness is greater than 20.

CONTACT SOLUTION

Having solved for the traction boundary value problem for a layered half-space, the normal contact problem may be solved by either of two approaches. In the first, by using the solution for $p(x) = \delta(x)$ and applying the contact boundary condition a singular integral equation can be derived which is solved numerically for the unknown pressure distribution in the contact zone[6]. In the second approach the unknown pressure is expanded in a series of basis functions, the coefficients of which are determined by considering a weak statement of the contact boundary condition[5]. We have chosen to follow the latter approach to solving the contact problem for the following reason. The pressure distribution under realistic indenters will be a relatively smooth function (such as a circular distribution for the case when a layer is not present), but the discretization procedure for the integral equation presented in Ref. [6] will still require a fairly large number of points to accurately represent such a function, and this situation becomes progressively worse for thin layers. Using the basis function approach is preferable, because the Hertz solution for the case when the layer and half-space elastic properties are the same provides a good first basis function, while a relatively small number of higher order basis functions (typically less than five) is needed to accurately represent smooth pressure distributions.

For the case of a rigid, cylindrical indenter contacting a layered half-space, the normal traction boundary condition on σ_{zz} at $z = 0$ is replaced by the mixed condition

$$w^{(1)}(x,0) - w^{(1)}(a,0) = W(x), |x| < a; \qquad \sigma_{zz}^{(1)}(x,0), |x| > a \tag{16}$$

where W is the prescribed relative displacement under the indenter (easily calculated knowing the shape of the indenter). A weak statement of this condition, is that the least-square error, $\mathscr{E}$, between the prescribed and actual displacement at the surface be minimized

$$\mathscr{E} = \int_{-a}^{a} (\delta w - W)^2 \, dx \tag{17}$$

where $\delta w(x) = w^{(1)}(x,0) - w^{(1)}(a,0)$. Next, the pressure distribution under the indenter is expanded in terms of a series of basis functions

$$p(x) = \sum_{i=1}^{N} a_i p_i(x). \tag{18}$$

Let $\delta w_i(x)$ be defined as the relative vertical surface displacement due to $p_i(x)$ acting alone. By linear superposition, the displacement can be expanded in terms of the δw_i

$$\delta w(x) = \sum_{i=1}^{N} a_i \delta w_i(x). \tag{19}$$

Substituting into eqn (17), and minimizing by setting the derivatives of $\mathscr{E}$ with respect to the unknown coefficients a_i to zero results in the least-squares normal equations for a_i

$$K\mathbf{a} = \mathbf{f} \tag{20}$$

where

$$K_{ij} = \int_{-a}^{a} \delta w_i w_j \, dx, \qquad f_i = \int_{-a}^{a} \delta w_i W \, dx. \tag{21}$$

After solving the coefficients, a_i, the pressure distribution under the indenter can be calculated from eqn (18). It is preferable to have the displacement basis functions δw_i orthogonal or nearly so to ensure well-conditioned normal equations. This is not possible because one first chooses the pressure basis functions p_i, and then solves for the δw_i numerically using the Fourier transform approach described above. In practice, however, we found that the following pressure basis function choice leads to well-conditioned normal equations so that their accurate solution is not a problem:

$$p_1(x) = \sqrt{\left(1 - \frac{x^2}{a^2}\right)}$$

$$p_i(x) = \cos\left(\frac{2i-3}{2} \cdot \frac{\pi x}{a}\right), \qquad i > 1. \tag{22}$$

The first basis function gives the exact Hertz solution for the case where the layer and substrate properties are identical.

The Fourier transform of each of the surface pressure functions in eqns (22) is determined analytically

$$\bar{p}_1 = \frac{\pi}{\omega} J_1(a\omega)$$

$$\bar{p}_i = \frac{\sin(\beta - \omega)a}{(\beta - \omega)} + \frac{\sin(\beta + \omega)a}{(\beta + \omega)}; \qquad \beta = \left(\frac{2i-3}{2}\right)\frac{\pi}{a}, \qquad i = 2, \ldots, N. \tag{23}$$

Equation (6) is then solved at a discrete number of frequencies for the unknown coefficients A_1, B_1, etc. Numerical inverse Fourier transformation is then performed for the surface displacements $\delta w_i(x)$.

Once the normal contact problem is solved, the pressure distribution on the boundary is known. The stresses at any point in the layer or half-space can then be determined from eqn (6) by numerical inverse Fourier transformation. For the case of fully-developed sliding contact, the pressure profile in the contact zone is assumed to be unaltered by the shearing tractions. This assumption becomes increasingly valid for higher values of Poisson's ratio and lower coefficients of friction[11], and is accurate for the numerical values used in this paper. The shear traction under the indenter is then given by $q(x) = fp(x)$ where f is the coefficient of friction of the indenter/layer interface. The stresses due to in-plane sliding contact are then solved for using eqns (6) via numerical inverse Fourier transformation, while the anti-plane shear stress in anti-plane sliding is solved for using eqns (10).

A computer program has been developed to implement the numerical approach described above. The program first solves the normal contact problem to determine the pressure profile under the indenter. The stresses at any point in the layer or substrate are then calculated for normal contact with either in-plane or anti-plane sliding. A complication is that the normal contact problem is geometrically nonlinear, because the contact zone size changes as the load increases. This is solved by an iterative approach where the contact half-width a is prescribed, and the mixed boundary problem (16) is then solved. The load is calculated from

$$L = \int_{-a}^{a} p(x) \, dx \tag{24}$$

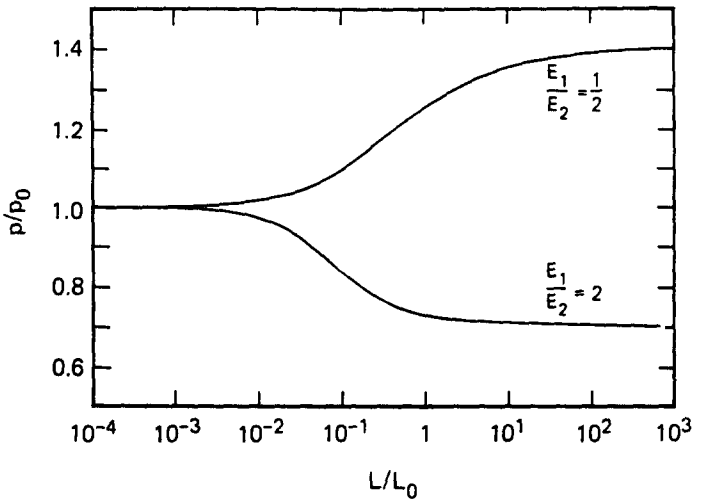

Fig. 2. Pressure under the center of the indenter as a function of applied load. $L_0 \equiv$ load corresponding to $a_0 = h$ for $E_1 = E_2$.

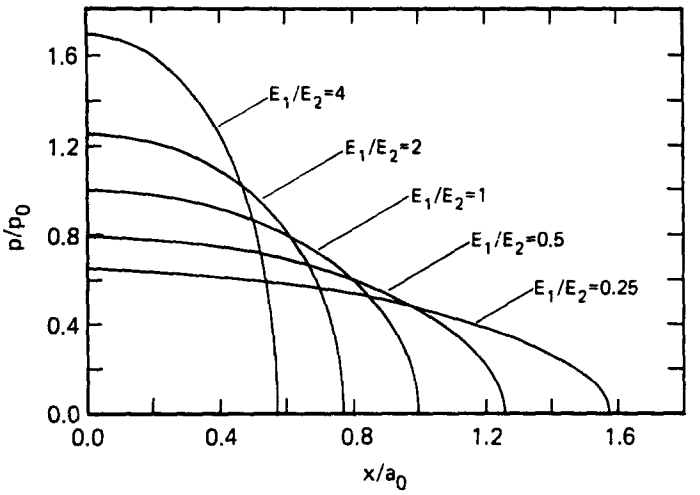

Fig. 3. Pressure profiles under the indenter for a layered medium.

where the pressure $p(x)$ is known from eqn (18). Given two values of contact width a_1 and a_2, with corresponding loads L_1 and L_2 that are below and above the desired load, L, a linear secant is used to determine the next estimate for a

$$a = (L - \beta)/\alpha \tag{25}$$

where $\alpha = (L_1 - L_2)/(a_1 - a_2)$ and $\beta = L_1 - \alpha a_1$. To start the iteration, two starting values of the contact width are needed that bracket the desired load. These are available from the Hertz solution. One value is determined from the Hertz solution for a half-space whose elastic properties are the same as those in the underlying half-space in the layered problem, while the other value is obtained from the Hertz solution for a half-space whose properties are the same as the layer material. This iterative procedure has been found in practice to converge rapidly.

RESULTS

The numerical solution of the sliding contact problem described above was first compared with cases for which exact solutions were available. For the normal contact case with the layer and substrate elastic properties equal the pressure profile agrees with the

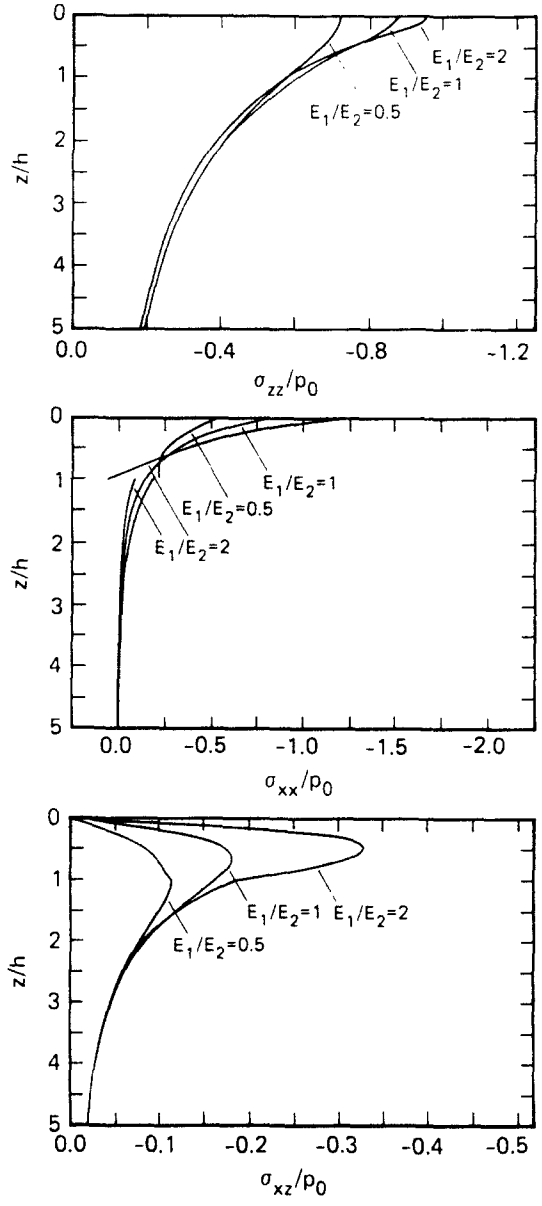

Fig. 4. Stress at $x = a_0/2$ under combined normal and in-plane sliding contact ($f = 0$).

Hertz solution, while in the sliding contact case the stresses under the indenter agreed with the exact solution presented by Hamilton and Goodman[2]. Letting the layer thickness tend to zero and infinity, respectively, the Hertz solution with appropriate elastic constants was recovered.

Results were next calculated for the layered case, using 0.3 for Poisson's ratio in both the layer and substrate. First, the pressure profile under the indenter was calculated for a wide range of applied loads. The pressure at the center of the indenter, normalized by the pressure from the Hertz solution (based on a half-space with properties the same as the layer) is shown in Fig. 2. For very small loads the presence of the substrate is not felt and the Hertz solution based on the layer properties is recovered, while for large loads the properties of the half-space dominate. Between these two asymptotic limits a smooth transition region exists. Next, a parameter study was performed on the effect of different layer and substrate stiffnesses on the pressure profile under the indenter (Fig. 3). The size of the contact zone and the pressure under the center of the indenter is quite different from the Hertzian case when E_1 differs significantly from E_2. Figures 2 and 3 agree with similar results in Ref. [6].

Next the stresses in the layer and substrate under the indenter were computed for

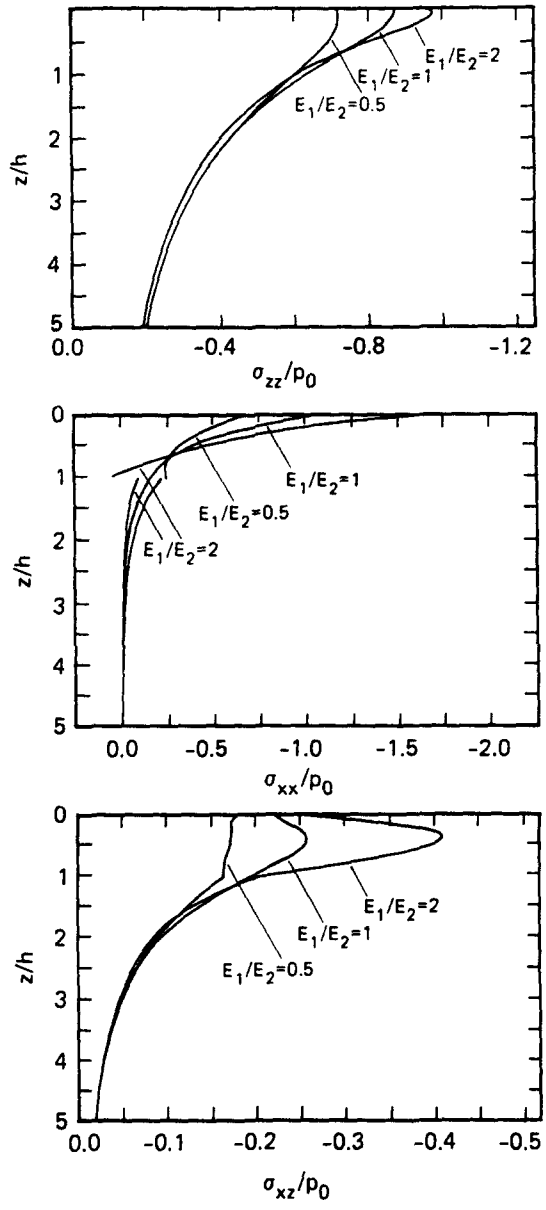

Fig. 5. Stress at $x = a_0/2$ under combined normal and in-plane sliding contact ($f = 0.25$).

normal contact with in-plane sliding. The load was set to the value L_0 which corresponds to $a_0/h = 1$ when $E_1 = E_2$, where a_0 is the contact zone half-width for the non-layered case. The three non-zero stress components σ_{xx}, σ_{zz}, and σ_{xz} are plotted as a function of depth at $x = a_0/2$, for values of the coefficient of friction $f = 0$, 0.25 and 0.5 (Figs 4–6). The maximum values of all three stress components increases when the layer is stiffer than the substrate. The stiffer layer behaves essentially as a beam attached to the half-space. Severe bending stress develops in the layer, resulting in an almost linear distribution of σ_{xx} through the layer. This stress component is tensile at the interface for a stiffer layer which is significant for cracks at the base of the layer and orthogonal to the interface. The shear stress at the interface is also aggravated by the stiffer layer. For layers that are more compliant than the substrate, both the maximum values of the stresses and the interfacial shear stress are reduced.

To investigate the influence of the layer on yielding in the layer or substrate, results for the Von Mises stress $\sqrt{J_2}/p_0$, where J_2 is the second invariant of the stress deviator tensor were next computed for the case $a_0/h = 1$. Contour plots are shown in Fig. 7 for the case where layer and substrate elastic properties are the same. The results in Fig. 7

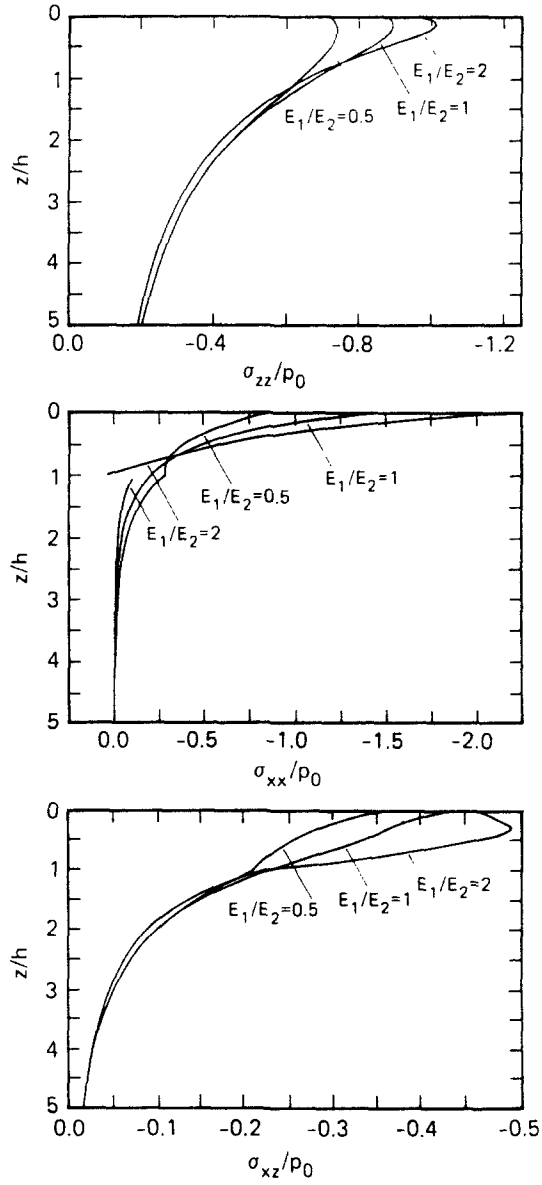

Fig. 6. Stress at $x = a_0/2$ under combined normal and in-plane sliding contact ($f = 0.5$).

agree with the non-layered solution presented in Ref. [2]. Contour plots for $E_1 = 2E_2$ are shown in Fig. 8. For this case the ratio of contact zone half-width to h is $a/h = 0.77$, and the presence of the stiffer layer severely distorts the contours with significant discontinuities occurring at the interface. For $f = 0$ the presence of the layer brings the point of maximum Von Mises stress close to the interface, and the maximum is 40% higher than in the non-layered case. For $f = 0.25$ the maximum stress moves closer to the surface compared to the non-layered case, and its value is also approximately 40% higher than in the non-layered case. For $f = 0.5$ the Von Mises stress is a maximum at the surface for both the layered and non-layered cases but its value is 52% higher in the non-layered case. Results for the maximum Von Mises stress under the indenter for $E_1 = 2E_2$ and $f = 0$ were computed for a wide range of a_0/h. It was found that the maximum is always in the layer. For $a_0/h \leq 0.7$, the maximum is above the interface, and above $a_0/h = 2.5$ the maximum position is at the surface. For intermediate a_0/h the maximum position is at the interface. In all cases the maximum value is greater than in the non-layered case.

Results for the case $E_1 = 0.5E_2$ are shown in Fig. 9. Here $a/h = 1.26$, and the maximum Von Mises stresses are approximately 20% lower than in a non-layered medium, and there

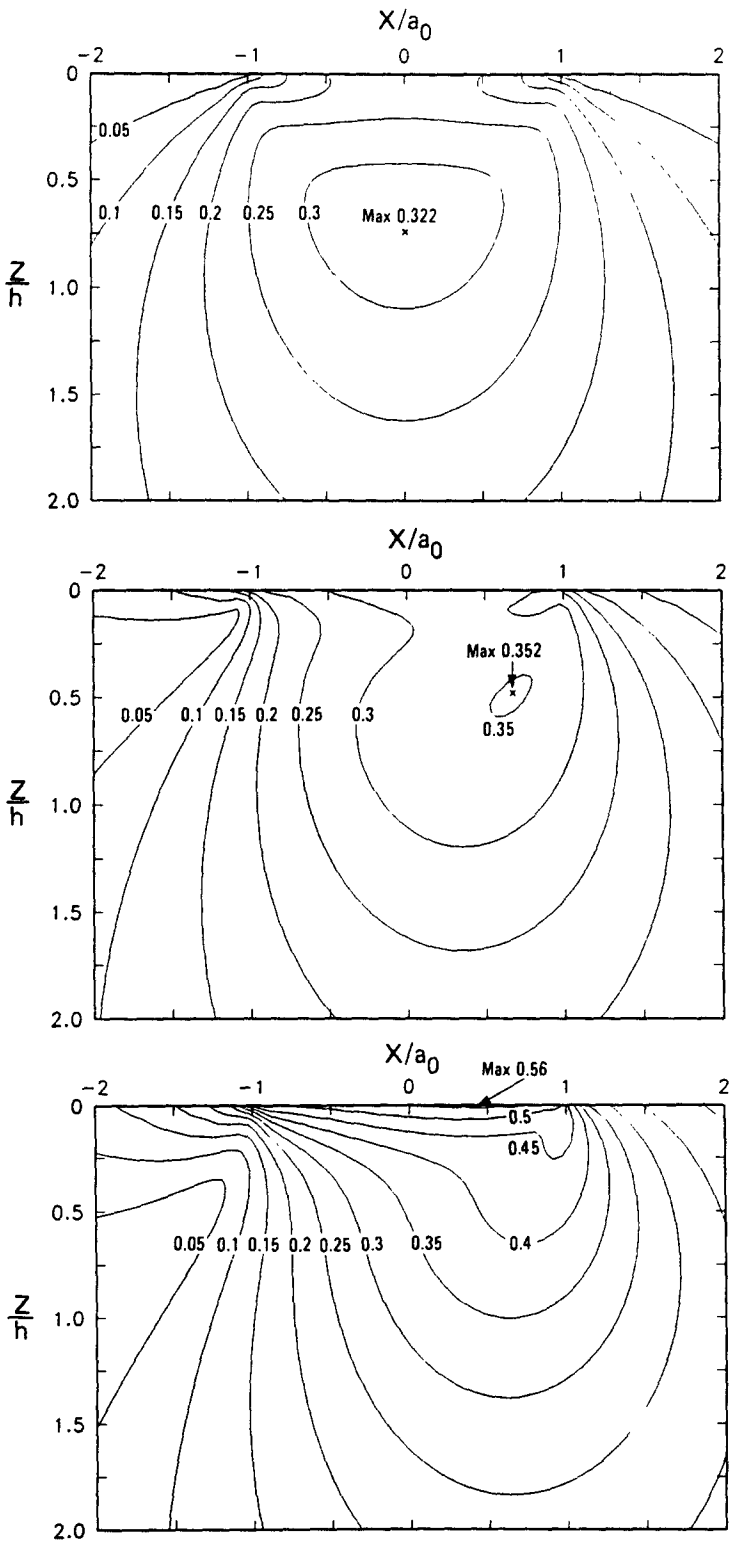

Fig. 7. Contour plots of $\sqrt{J_2}/p_0$ for $E_1 = E_2$. (a) $f = 0$, (b) $f = 0.25$, (c) $f = 0.5$.

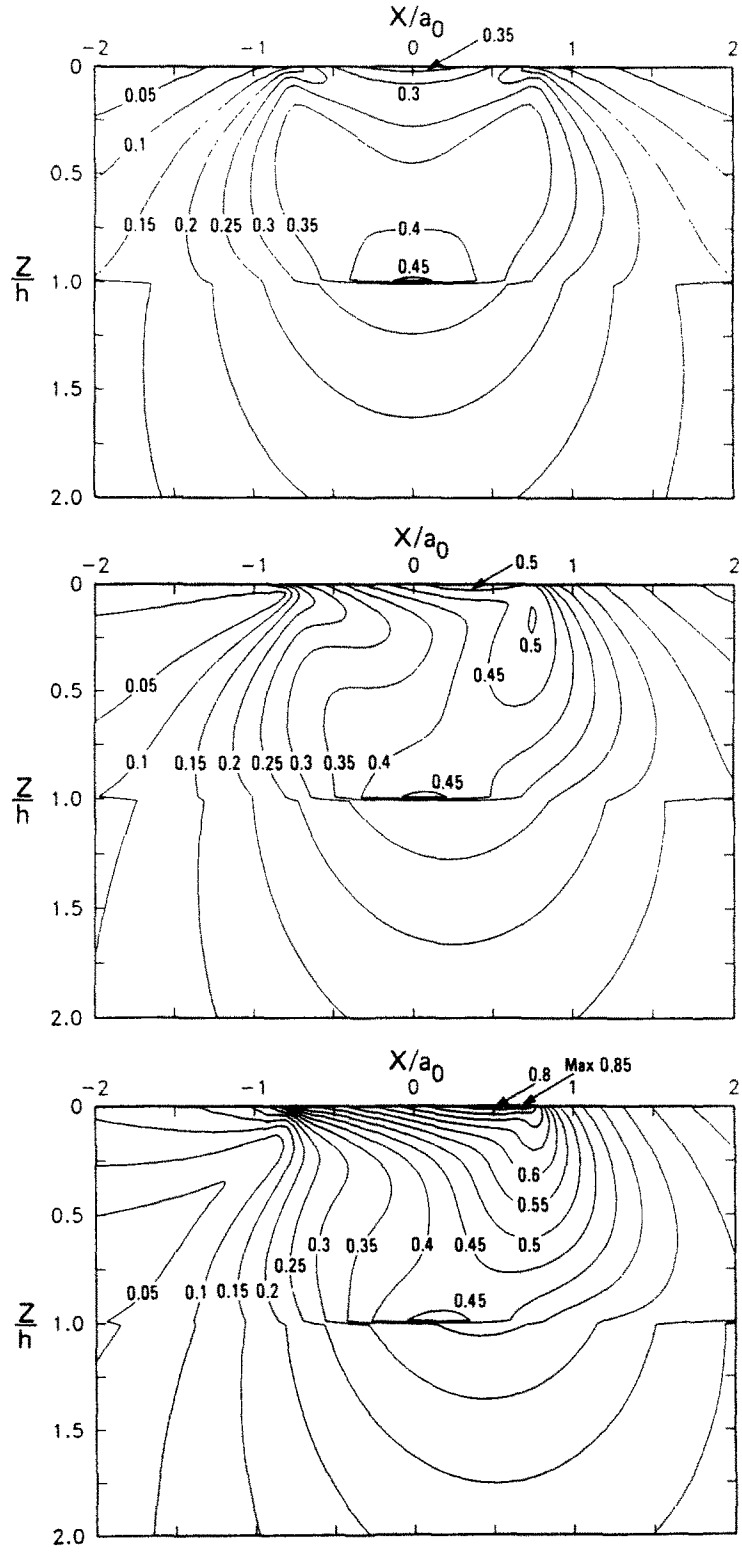

Fig. 8. Contour plots of $\sqrt{J_2}/p_0$ for $E_1 = 2E_2$. (a) $f = 0$, (b) $f = 0.25$, (c) $f = 0.5$.

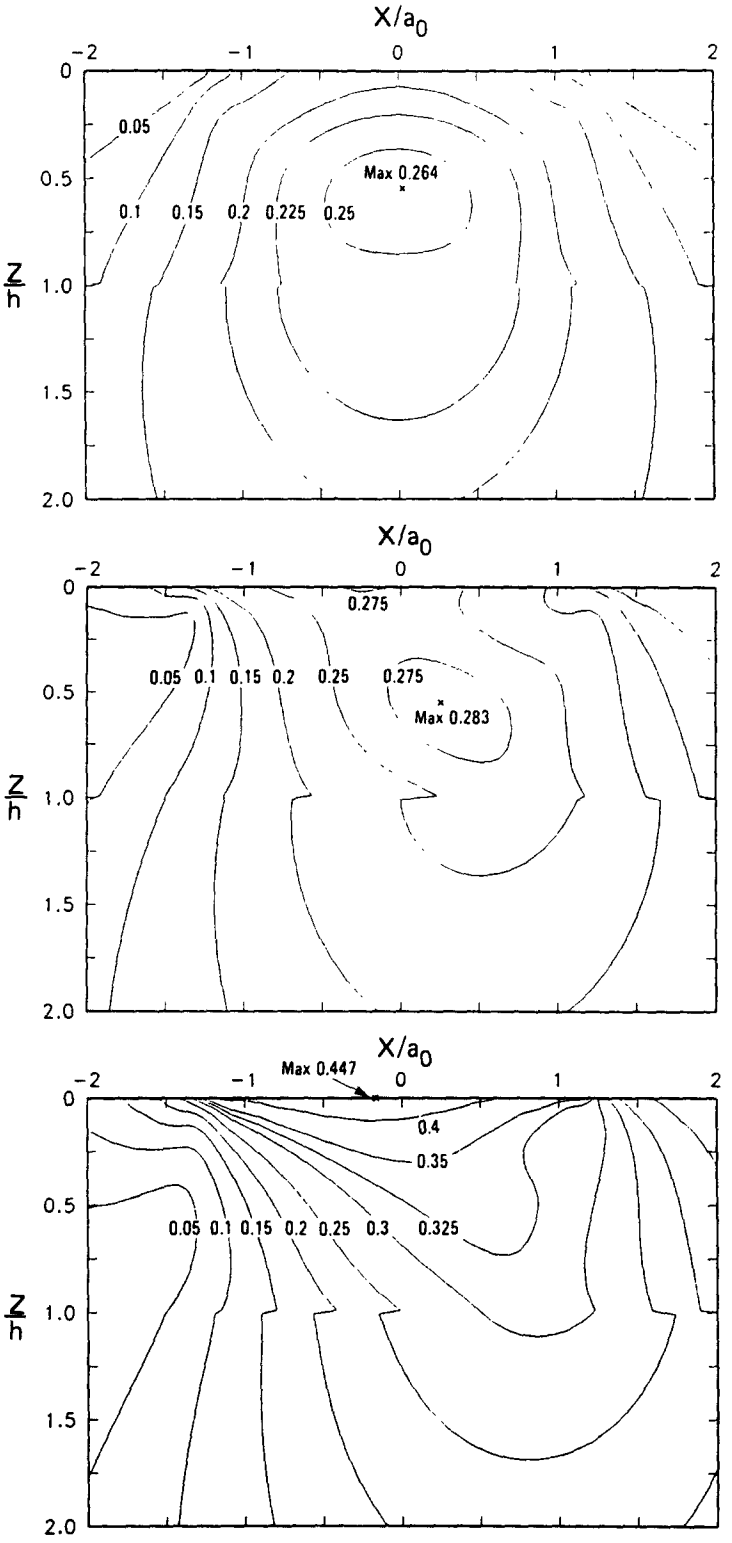

Fig. 9. Contour plots of $\sqrt{J_2}/p_0$ for $E_1 = 1/2E_2$. (a) $f = 0$, (b) $f = 0.25$, (c) $f = 0.5$.

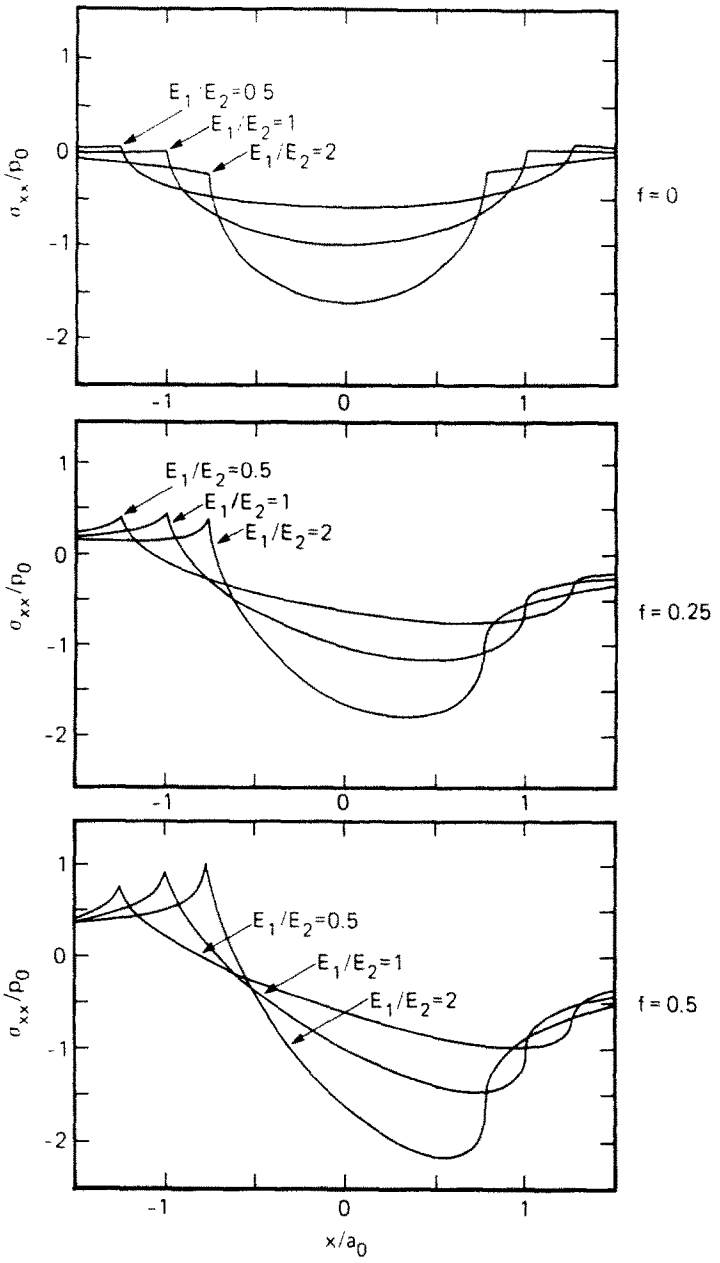

Fig. 10. σ_{xx} on the surface at $x = 0$. (a) $f = 0$, (b) $f = 0.25$, (c) $f = 0.5$.

is only a mild discontinuity at the interface. Results for the maximum Von Mises stress under the indenter for $E_1 = 0.5E_2$ and $f = 0$ were computed for various values of a_0/h, and the maximum was always found to be less than in the non-layered case. The maximum is in the layer for $a_0/h \leq 1.5$ and in the substrate for $a_0/h \geq 1.5$. The point of maximum $\sqrt{J_2}$ is not the point of maximum tensile principal stress of the sliding contact cases studied. The tensile stress tends to be highest near the surface at the rear edge of the contact zone.

Because layer materials can be brittle and contain surface defects, the influence of the layer elastic stiffness on the tensile stress on the surface is of interest. Results for σ_{xx} on the surface at $x = 0$ are shown in Fig. 10 for $f = 0$, 0.25, and 0.5. Increasing the coefficient of friction dramatically increases the maximum tensile stress on the surface for the values of E_1 and E_2 studied. A similar effect was previously reported for spherical contact on a non-layered medium[2]. At the higher coefficients of friction it is beneficial to have a more compliant coating while the opposite is true for lower coefficients of friction.

The contact stress analysis was next performed for the case of a thin layer, $h = a_0/20$.

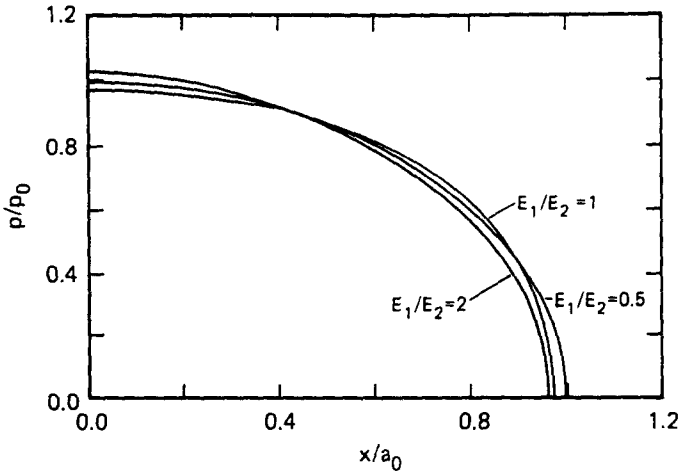

Fig. 11. Pressure profile under the indenter for a layered medium, $a_0/h = 20$.

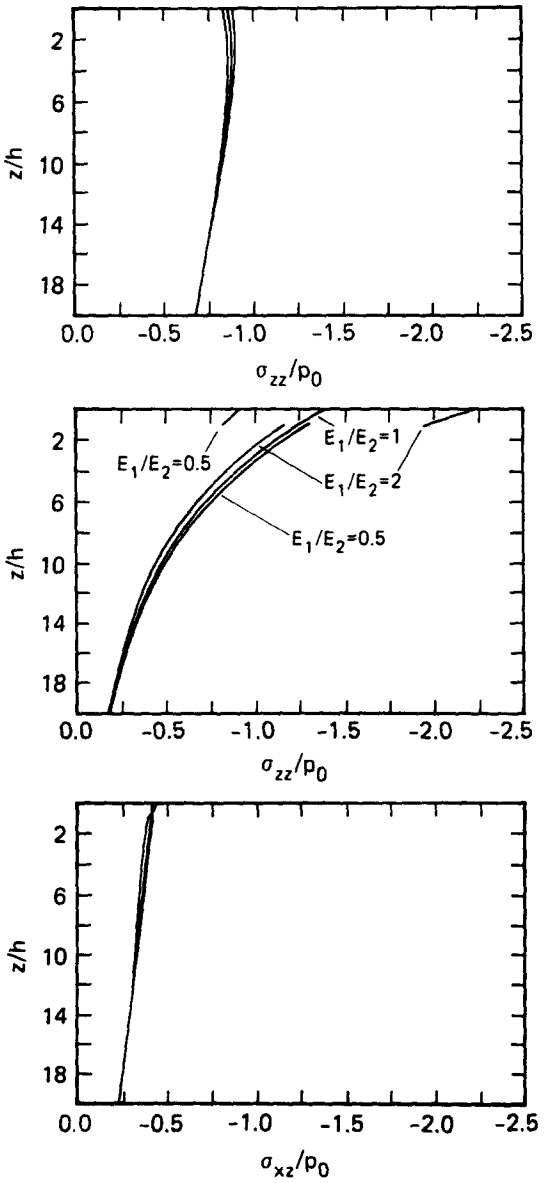

Fig. 12. Stress under indenter at $x = a/2$ for $a_0/h = 20$ and $f = 0.5$.

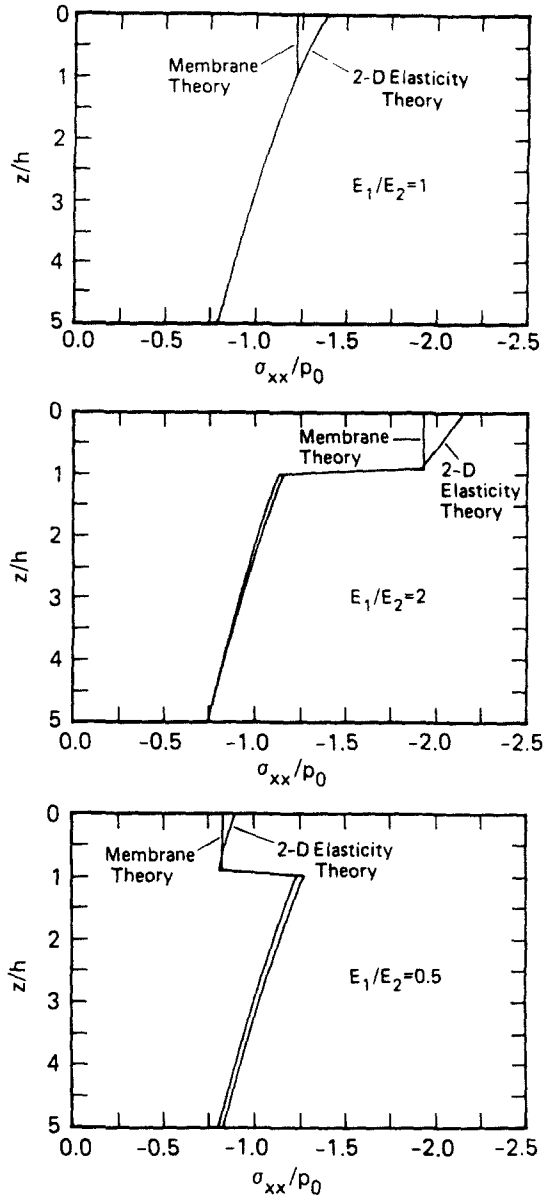

Fig. 13. Comparison of elasticity and membrane theories for σ_{xx} for $a/h = 20$.

The stiffness of the layer does not significantly affect the pressure profile here (Fig. 11). Results for all three non-zero stress components are shown in Fig. 12 for $f = 0.5$. The values of σ_{zz} and σ_{xz} do not differ appreciably from the non-layered case, while the ratio E_1/E_2 dramatically affects the value of σ_{xx} in the layer. The membrane theory discussed above was next applied to this situation. Results for σ_{xx} are shown in Fig. 13 and contrasted with the elasticity solution. The membrane theory agrees well with the elasticity solution for the value of σ_{xx} at the interface but deviates at the surface because the flexural stiffness of the layer is neglected. The membrane theory is accurate for large values of a/h and may easily be extended to multiple layers.

In the anti-plane sliding contact problem, the values of σ_{zz} and σ_{xx} are the same as in the normal contact situation. The out-of-plane shear stress, σ_{zy} under the indenter due to anti-plane sliding is presented in Fig. 14, for the case of $a_0 = h$. The maximum value of σ_{zy} increases when the layer is stiffer than the half-space.

The results presented show that the stiffness of the layer relative to the substrate has a strong influence on the potential for yielding in both the layer and substrate and on the adhesion failure of the interface between them, and that in general for a fixed value of

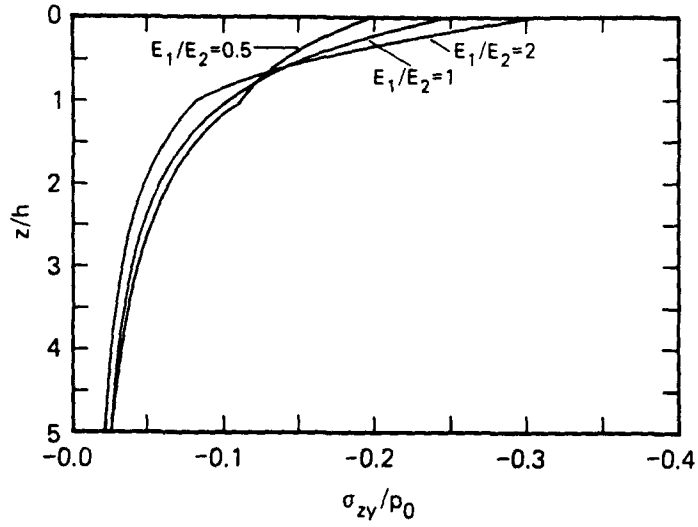

Fig. 14. Shear stress under the indenter for combined normal and anti-plane sliding contact ($f = 0.5$).

substrate stiffness the stress state is aggravated by increasing the layer stiffness. These results can also be used to study in a qualitative manner the significance of cracks in the layer and at the interface. By modified application of the theory presented in Ref. [12] the crack driving force for delamination cracks at the interface under a compressive stress σ_{xx} can be calculated.

REFERENCES

1. H. Poritsky, *J. Appl. Mech.* **18**, 191 (1950).
2. G. M. Hamilton and L. E. Goodman, *J. Appl. Mech.* **33**, 371 (1966).
3. D. M. Burmister, *J. Appl. Phys.* **16**, 89 (1945).
4. W. T. Chen, *Int. J. Engng Sci.* **9**, 775 (1971).
5. W. T. Chen and P. Engel, *Int. J. Solids Structures* **8**, 1257 (1972).
6. P. K. Gupta and J. A. Walowit, *Trans. ASME, J. Lub. Tech.* 250 (April 1974).
7. Y. O. Tu, *J. Appl. Mech.* **35**, 283.
8. P. K. Gupta, J. A. Walowit and E. F. Finkin, *Trans. ASME, J. Lub. Tech.* 427 (October 1973).
9. I. S. Sokolnikoff, *Mathematical Theory of Elasticity*. McGraw-Hill, New York (1956).
10. K. Nikpur and R. Gohar, *Tribology* **8**, 2 (1975).
11. Ye. A. Kuznetsov, *Wear* **50**, 183 (1978).
12. A. Evans and J. Hutchinson, *Int. J. Solids Structures* **20**, 455 (1984).